# The electronic spectrum of $NiTa_2O_6$

R. Borromei, E. Cavalli and L. Oleari*
*Istituto di Chimica Fisica, Università di Parma, viale delle Scienze 85, Parma (Italy)*

(Received June 15, 1992)

**Abstract**

The polarized absorption spectrum of single crystals of $NiTa_2O_6$ has been measured from 6000 to 28 000 $cm^{-1}$ at various temperatures from 300 to 10 K. All the observed absorption regions are due to electronic transitions mainly localized on the $Ni^{2+}$ ions. The first band system in the region 6000–10 500 $cm^{-1}$ corresponds to a transition which occurs mainly by magnetic dipole mechanism. The band systems in the other regions are due to vibronic transitions. By applying our method of analysis of the site geometry based on symmetry descent, we deduce that the $O_h \rightarrow D_{2h}$ distortion of $NiO_6^{n-}$ can be decomposed into two contributions related to the steps $O_h \rightarrow D_{4h}$ and $D_{4h} \rightarrow D_{2h}$ and that the second contribution is much larger than the first. Successively we give an explanation for most of the features of the spectra by considering only the $D_{4h} \rightarrow D_{2h}$ perturbation and the vibronic interactions. The effect of the spin–orbit coupling has also been considered.

## Introduction

This work is part of a systematic investigation we are carrying out on the optical properties of the $Ni^{2+}$ ions in crystals with a distorted octahedral coordination of oxygen atoms [1–4].

The main purpose of this paper is the interpretation of the low temperature absorption spectra of $NiTa_2O_6$ crystals by applying our procedure [5] of analysis of the sites of the $Ni^{2+}$ ions in terms of 'symmetry descent'. In fact such procedure is particularly suitable because it allows a rigorous and quantitative decomposition of the distortion of the oxygen coordination sphere into a set of contributions of different symmetry and a parallel decomposition of the Hamiltonian. The method has been already applied successfully in our previous work on $LiNiPO_4$ [4].

As is well known in systems where the distortion removes the centre of symmetry, the predominant mechanism of the electronic transitions is often that of electric dipole and the related moments are different from zero mainly because of the distortion. Conversely in systems where the distortion does not remove the symmetry centre other mechanisms, like the vibronic and/or the magnetic dipole ones, have to be considered. This point is at the basis of our interest in $NiTa_2O_6$ where the $Ni^{2+}$ sites have a centre of symmetry. This interest is also supported by the observation of Ferguson *et al.* [6] that in $MgF_2$ 'doped' with $Ni^{2+}$, where the $Mg^{2+}$ site symmetry is equal to that of $Ni^{2+}$ in $NiTa_2O_6$, the transition mechanism of the first electronic band is mostly that of magnetic dipole.

*Author to whom correspondence should be addressed.

## Experimental

Green single crystals of $NiTa_2O_6$ were grown by means of the flux-growth technique. Mixtures of composition 8.2 wt.% NiO, 48.5 wt.% $Ta_2O_5$ and 43.3 wt.% $Na_2B_4O_7$ were placed in tightly covered 50 $cm^3$ platinum crucibles and heated to 1400 °C in a furnace. After a period of soaking, crystals were grown by slow cooling down to 750 °C. The crystals were separated from the borate flux by leaching with a dilute solution of HCl.

The orientation of the crystals was first found optically with a microscope and then checked by X-ray diffraction.

The spectra were recorded at various temperatures from room temperature to 10 K with a spectrophotometric system consisting of a SPEX 1.26 m f/9 Czerny-Turner monochromator and a recording system connected to a PC computer. The detectors were a RCA C31034 phototube for the UV–Vis region and a PbS N.E.P. cell for the near-IR. The cryostat was an equipment 'Air Products Displex DE 202' closed cycle.

## Results and discussion

### *Crystal structure*

The crystal structure of $NiTa_2O_6$ is well known and is reported in ref. 7. The crystal is tetragonal

0020-1693/93/$6.00

($P4_2/mnm$) with two $NiO_6^{n-}$ units per cell. The units are equal as regards their geometry but have different orientations (Fig. 1). Each unit $NiO_6^{n-}$ has a distorted octahedral geometry with an actual symmetry $D_{2h}$. One of the three binary axes (i.e. $z'$) passes through two oxygen atoms (O(5) and O(6)). The other binary axes bisect the angles between the oxygen atoms on the plane orthogonal to $z'$ (Fig. 2). The latter (O(1), O(2), O(3), O(4)) form a rectangle with the longer edges (O(2)–O(3) and O(1)–O(4)) parallel to the crystallographic $c(=x')$ axis. The Ni–O distance varies only slightly from the oxygens on the $z'$ axis (2.050 Å) to those of the $x'y'$ plane (2.084 Å). The distortion concerns mainly the angles between the oxygens on the $x'y'$ plane (O(1)NiO(2) = 81.15°, O(2)NiO(3) = 98.85°).

It is worth pointing out that the shortest distance between the $Ni^{2+}$ ions lying on the plane orthogonal to the $c$ axis is 4.722 Å and that between the $Ni^{2+}$ ions belonging to adjacent planes is 5.664 Å. Moreover experimental measurements on the magnetic properties of $NiTa_2O_6$ [8] have shown that there is a long-range antiferromagnetic ordering only at $T_c = 10.3$ K. The broad maximum in the magnetic susceptibility above $T_c$ has to be attributed only to low-dimensional short-range magnetic ordering. This means that the magnetic interaction among the $Ni^{2+}$ ions is rather weak.

On the basis of these facts we thought it reasonable to carry out an interpretation of the electronic spectra by considering first the transitions as localized on single $NiO_6^{n-}$ units.

*Electronic structure of the $NiO_6^{n-}$ units and the various perturbations*

For the interpretation of the spectra we have adopted the procedure proposed in ref. 5 based on symmetry descent. Specifically we have considered the path $O_h \rightarrow D_{4h} \rightarrow D_{2h}$. In this regard it has to be pointed out that in the first step $O_h \rightarrow D_{4h}$ there is only one symmetry species which becomes totally symmetric in $D_{4h}$, i.e. $E_g(z^2)$, and similarly in the step $D_{4h} \rightarrow D_{2h}$ there is only the species $T_{2g}(xy)$. By using the $O_h$ symmetry coordinates reported in ref. 5 for each $NiO_6^{n-}$ unit only three of these coordinates are not zero*

$$S(A_{1g}) = \frac{1}{\sqrt{6}}(x_1 + y_2 - x_3 - y_4 - z_5 + z_6) = \sqrt{6} l_{M-O} = 5.067 \text{ Å}$$

$$S(E_g, z^2) = \frac{1}{2\sqrt{3}}(-x_1 - y_2 + x_3 + y_4 - 2z_5 + 2z_6) = -0.032 \text{ Å}$$

$$S(T_{2g}, xy) = \frac{1}{2}(y_1 + x_2 - y_3 - x_4) = 0.322 \text{ Å}$$

This means that the system can be represented by a regular octahedron with Ni–O distance $l_{M-O} = 1/\sqrt{6}\, S(A_{1g}) = 2.069$ Å and two successive distortions related to the symmetry descent-steps $O_h \rightarrow D_{4h}$ and $D_{4h} \rightarrow D_{2h}$. The first distortion $O_h \rightarrow D_{4h}$ is associated with the coordinate $S(E_g, z^2)$, and the second one $D_{4h} \rightarrow D_{2h}$ with the coordinate $S(T_{2g}, xy)$.

In connection with this picture the Hamiltonian can be decomposed as

$$\hat{H} = \hat{H}^0 + \hat{H}(E_g, z^2) + \hat{H}(T_{2g}, xy)$$

where $\hat{H}^0$ is related to the undistorted octahedron, $\hat{H}(E_g, z^2)$ and $\hat{H}(T_{2g}, xy)$ to the corresponding distortions $O_h \rightarrow D_{4h}$ and $D_{4h} \rightarrow D_{2h}$. Considering the d-type molecular orbitals $t_{2g,r}$ $(r = yz, xz, xy)$ and $e_{g,s}$ $(s = z^2, x^2 - y^2)$, we can write the following matrices as representative of the distortions

| | | $O_h \rightarrow D_{4h}$ | | | | | $D_{4h} \rightarrow D_{2h}$ | | | | |
|---|---|---|---|---|---|---|---|---|---|---|---|
| $t_{2g}$ | $yz$ | $-\eta$ | 0 | 0 | 0 | 0 | 0 | $\vartheta$ | 0 | 0 | 0 |
| | $xz$ | 0 | $-\eta$ | 0 | 0 | 0 | $\vartheta$ | 0 | 0 | 0 | 0 |
| | $xy$ | 0 | 0 | $2\eta$ | 0 | 0 | 0 | 0 | 0 | $\zeta$ | 0 |
| $e_g$ | $z^2$ | 0 | 0 | 0 | $-\epsilon$ | 0 | 0 | 0 | $\zeta$ | 0 | 0 |
| | $x^2-y^2$ | 0 | 0 | 0 | 0 | $\epsilon$ | 0 | 0 | 0 | 0 | 0 |

where

*We choose as reference frame a cartesian axis system with origin on the metal ($x_M = y_M = z_M = 0$) and orientation such that $S(T_{1g}, R_x) = S(T_{1g}, R_y) = S(T_{1g}, R_z) = 0$. Moreover with regard to the $D_{2h}$ symmetry we assume as principal two-fold axis the axis passing through the oxygen atoms O(5) and O(6) (i.e. $z'$). This convention is different from that of ref. 6.

$\hat{H}(E_g, z^2) = \sum_i \hat{h}_i(E_g, z^2)$ $\quad \hat{H}(T_{2g}, xy) = \sum_i \hat{h}_i(T_{2g}, xy)$ $\quad \hat{h}_i(\,) =$ one-electron operator

$$\eta = \frac{1}{2}\langle t_{2g}, xy|\hat{h}(E_g, z^2)|t_{2g}, xy\rangle = -\langle t_{2g}, yz|\hat{h}(E_g, z^2)|t_{2g}, yz\rangle = -\langle t_{2g}, xz|\hat{h}(E_g, z^2)|t_{2g}, xz\rangle$$

$$\epsilon = -\langle e_g, z^2|\hat{h}(E_g, z^2)|e_g, z^2\rangle = \langle e_g, x^2-y^2|\hat{h}(E_g, z^2)|e_g, x^2-y^2\rangle$$

$$\vartheta = \langle t_{2g}, yz|\hat{h}(T_{2g}, xy)|t_{2g}, xz\rangle \qquad \zeta = \langle t_{2g}, xy|\hat{h}(T_{2g}, xy)|e_g, z^2\rangle$$

In Fig. 3 we give a scheme of the trend of the molecular orbital energies along the symmetry descent, where

$$1a_g = N[1a_g^0 + \lambda 2a_g^0] \qquad 2a_g = N[2a_g^0 - \lambda 1a_g^0]$$

$$b_{2g} = \frac{1}{\sqrt{2}}[t_{2g,yz} + t_{2g,xz}] \qquad b_{1g} = e_{g,x^2-y^2}$$

$$b_{3g} = \frac{1}{\sqrt{2}}[t_{2g,yz} - t_{2g,xz}]$$

$$1a_g^0 = t_{2g,xy} \qquad 2a_g^0 = e_{g,z^2} \qquad \omega \approx \frac{\zeta^2}{\Delta - \epsilon - 2\eta}$$

$\lambda =$ coefficient $\qquad N = (1+\lambda^2)^{-1/2} =$ normalization factor

With regard to the $Ni^{2+}$ ion in octahedral symmetry it is known that the ground state is $^3A_{2g}(0)$. The possible ligand field excited states are $^3T_{2g}(1)$, $^3T_{1g}(1)$, $^1E_g(0)$, $^1T_{2g}(1)$, $^3T_{1g}(2)$, $^1A_{1g}(0)$, $^1T_{1g}(1)$, $^1E_g(1)$, $^1T_{2g}(2)$, $^1A_{1g}(2)$ according to increasing energy in the Tanabe–Sugano diagram when $\Delta/B < 10$. The preponderant configuration is given in brackets: in particular with 0, 1 and 2 we denote $t_{2g}^6e_g^2$, $t_{2g}^5e_g^3$ and $t_{2g}^4e_g^4$, respectively.

Under the perturbations related to the distortions $O_h \to D_{4h}$ and $D_{4h} \to D_{2h}$ and the spin–orbit coupling $D_{2h} \to D_{2h}^*$ the degeneracies of the levels are removed according to Fig. 9.

Since $|S(E_g, z^2)| \ll |S(T_{2g}, xy)|$, we have to expect that in parallel the perturbation associated with the distortion $D_{4h} \to D_{2h}$ has a major role with respect to $O_h \to D_{4h}$.

In $D_{2h}$ symmetry the $O_h$ states subdivide as follows

| $O_h$ | $D_{2h}$ |
|---|---|
| $^3A_{2g}$ | $^3B_{1g}$ |

$$^{1,3}T_{2g} \begin{cases} ^{1,3}A_g = {}^{1,3}T_{2g}(xy) \\ ^{1,3}B_{2g} = \frac{1}{\sqrt{2}}\{{}^{1,3}T_{2g}(yz) + {}^{1,3}T_{2g}(xz)\} \\ ^{1,3}B_{3g} = \frac{1}{\sqrt{2}}\{{}^{1,3}T_{2g}(yz) - {}^{1,3}T_{2g}(xz)\} \end{cases}$$

$$^{1,3}T_{1g} \begin{cases} ^{1,3}B_{1g} = {}^{1,3}T_{1g}(z) \\ ^{1,3}B_{2g} = \frac{1}{\sqrt{2}}\{-{}^{1,3}T_{1g}(x) + {}^{1,3}T_{1g}(y)\} \\ ^{1,3}B_{3g} = \frac{1}{\sqrt{2}}\{{}^{1,3}T_{1g}(x) + {}^{1,3}T_{1g}(y)\} \end{cases}$$

$$^1E_g \begin{cases} ^1A_g = {}^1E_g(z^2) \\ ^1B_{1g} = {}^1E_g(x^2-y^2) \end{cases}$$

Here we report only the ligand field matrices related to the triplet states in the case of $D_{2h}$ symmetry with $\eta$ and $\epsilon$ neglected. Later on we shall examine these matrices as a basis for the interpretation of the spectra.

$$
\begin{array}{cc|ccc|}
 & & {}^3A_g & {}^3T_{2g}(1)\,|\Delta| & \\
{}^3B_{1g} & {}^3A_{2g}(0) & 0 & -\zeta & 0 \\
 & {}^3T_{1g}(1) & -\zeta & \Delta+12B & 6B \\
 & {}^3T_{1g}(2) & 0 & 6B & 2\Delta+3B
\end{array}
$$

$$
\begin{array}{cc|ccc|}
 & & {}^3T_{2g}(1) & {}^3T_{1g}(1) & {}^3T_{1g}(2) \\
{}^3B_{2g} & {}^3T_{2g}(1) & \Delta+\frac{1}{2}\vartheta & -\frac{\sqrt{3}}{2}\vartheta & \frac{1}{2}\zeta \\
 & {}^3T_{1g}(1) & -\frac{\sqrt{3}}{2}\vartheta & \Delta+12B-\frac{1}{2}\vartheta & 6B+\frac{\sqrt{3}}{2}\zeta \\
 & {}^3T_{1g}(2) & \frac{1}{2}\zeta & 6B+\frac{\sqrt{3}}{2}\zeta & 2\Delta+3B-\vartheta
\end{array}
$$

$$
\begin{array}{cc|ccc|}
 & & {}^3T_{2g}(1) & {}^3T_{1g}(1) & {}^3T_{1g}(2) \\
{}^3B_{3g} & {}^3T_{2g}(1) & \Delta-\frac{1}{2}\vartheta & \frac{\sqrt{3}}{2}\vartheta & -\frac{1}{2}\zeta \\
 & {}^3T_{1g}(1) & \frac{\sqrt{3}}{2}\vartheta & \Delta+12B+\frac{1}{2}\vartheta & 6B-\frac{\sqrt{3}}{2}\zeta \\
 & {}^3T_{1g}(2) & -\frac{1}{2}\zeta & 6B-\frac{\sqrt{3}}{2}\zeta & \Delta+3B+\vartheta
\end{array}
\qquad (1)
$$

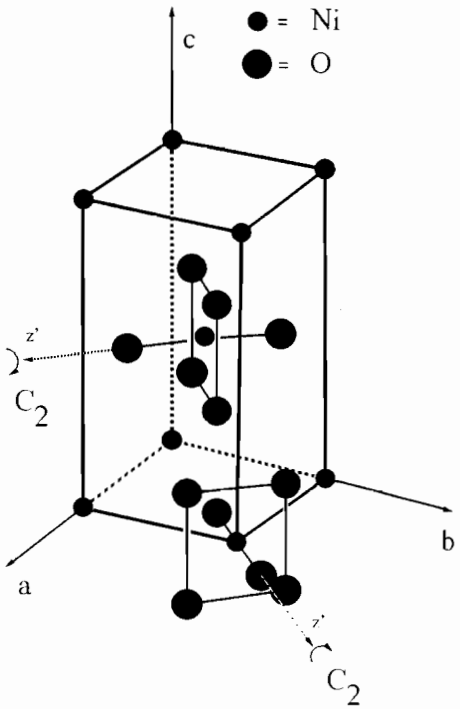


Fig. 1. The orientation of the $NiO_6^{n-}$ groups in the unit cell.

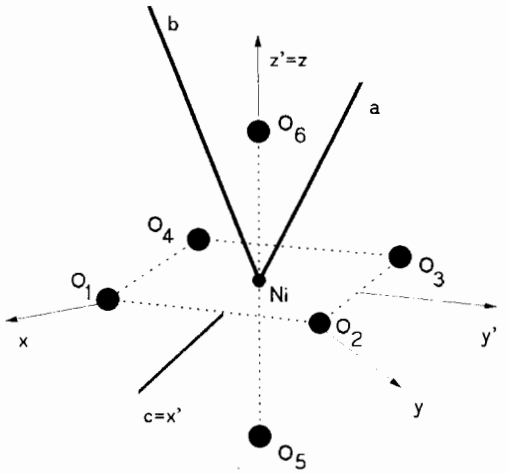


Fig. 2. Cartesian axes: $x$, $y$, $z$ in $O_h$ symmetry: $x'$, $y'$, $z'$ in $D_{2h}$; ($a$, $b$, $c$) crystallographic axes.

*Description of the spectra*

The $\alpha$, $\sigma$ and $\pi$ [6, 9] spectra have been recorded from two different crystals.

Experimentally all the range 6000–28 000 $cm^{-1}$ has been examined. We have observed three absorption regions relatively more intense (Figs. 4, 5, 6) and one weaker (Fig. 7). Each region appears as a set of more or less overlapping bands which we shall call band systems. In each system there is evidence of several components and a fine structure. The main features are reported in Table 1.

All the band systems present a remarkable increasing intensity and merging of the components with an increase of the temperature. However the first system (6000–10 500 $cm^{-1}$) quite differently from the others does not change significantly in intensity from 10 up

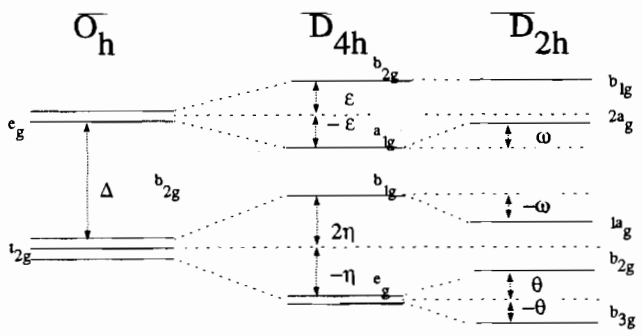


Fig. 3. MO energy level scheme.

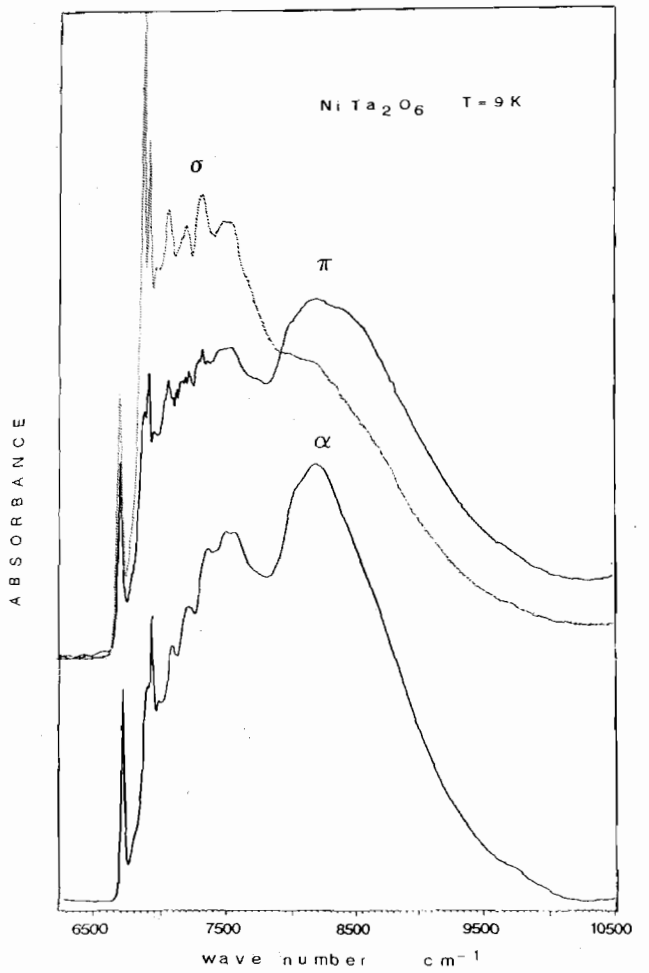


Fig. 4. First intense band system.

to 50 K, except for the peaks at 6720, 6900 and 6935 $cm^{-1}$ which change in shape.

The $\alpha$ spectrum of the first band system is rather close to the $\pi$ one and different from $\sigma$. Conversely the $\alpha$ spectrum of the other systems is more similar to the $\sigma$ one and different from $\pi$. These facts prove inequivocally that the predominant mechanism is that of magnetic dipole in the first band system and that of electric dipole with vibronic coupling in the others.

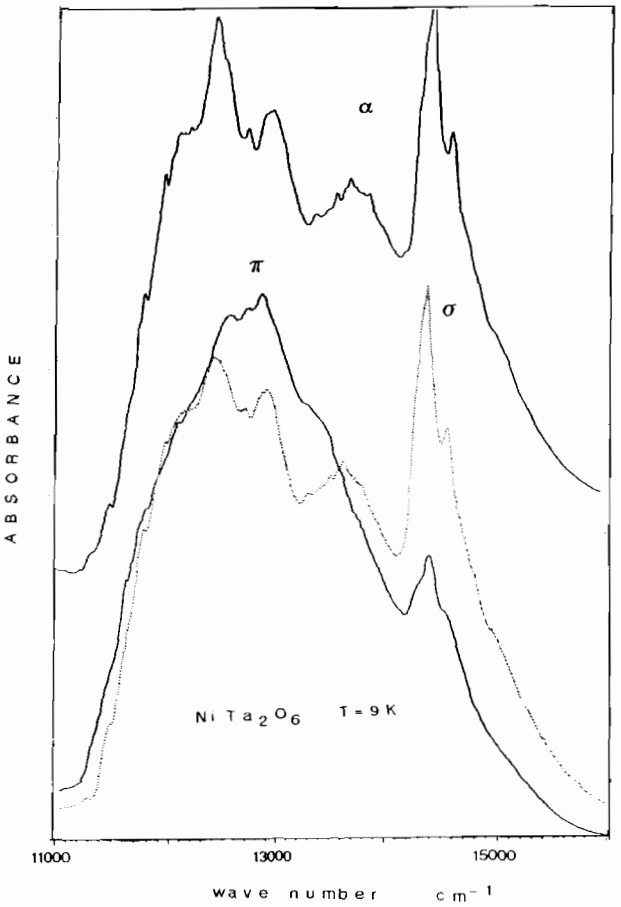


Fig. 5. Second intense band system.

Finally we have to remark that the overall intensity of the spectra is much weaker as compared to that of similar crystal systems containing $Ni^{2+}$ ions in sites lacking a symmetry centre [1, 2, 4].

*Interpretation of the spectra*

As a first approach an interpretation can be given in $O_h$ symmetry by assigning the three relatively more intense band systems (Figs. 4–6) to transitions to the three triplet states $^3T_{2g}(1)$, $^3T_{1g}(1)$, $^3T_{1g}(2)$. In fact a good fit to the centres of such band systems can be obtained with a ligand field calculation with $10Dq = 7600$ $cm^{-1}$ and $B = 850$ $cm^{-1}$. Moreover with these values of $10Dq$ and $B$ and assuming $C/B = 4.38$ we have that the peaks at 14 400–14 580 $cm^{-1}$ correspond to $^1E_g(0) \leftarrow {}^3A_{2g}(0)$, the weak band at 19 800–21 400 $cm^{-1}$ to $^1T_{2g}(1) \leftarrow {}^3A_{2g}(0)$ and the weak peak at 21 750 $cm^{-1}$ to $^1A_{1g}(0) \leftarrow {}^3A_{2g}(0)$ (column $A_2$ of Table 3).

Before proceeding to examine the details of the band systems, the following points have to be considered.

The spin–orbit coupling in the $Ni^{2+}$ ions is not negligible and we should examine the splitting of the levels on the basis of the double group $D^*_{2h}$ (Fig. 9). Since the number of the possible transitions to be

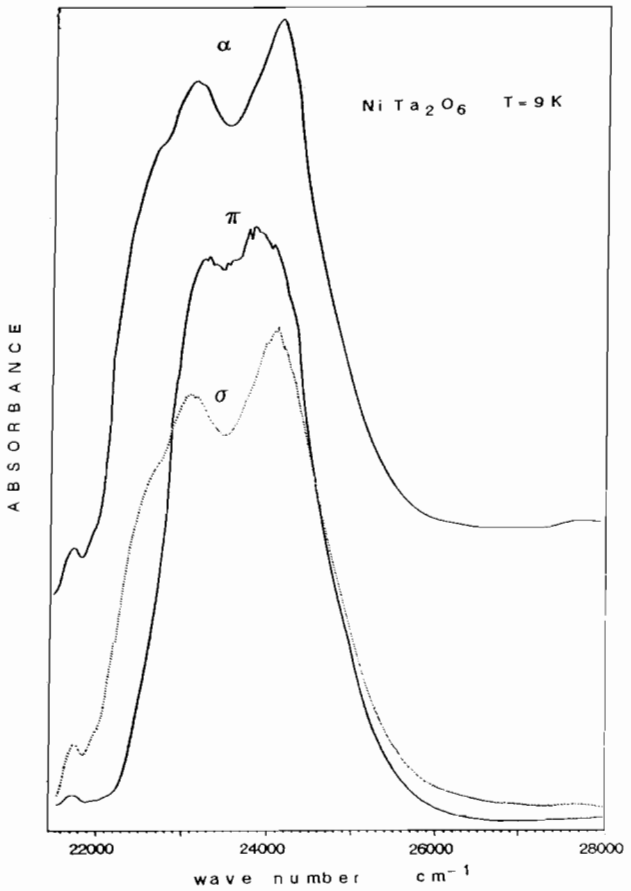


Fig. 6. Third intense band system.

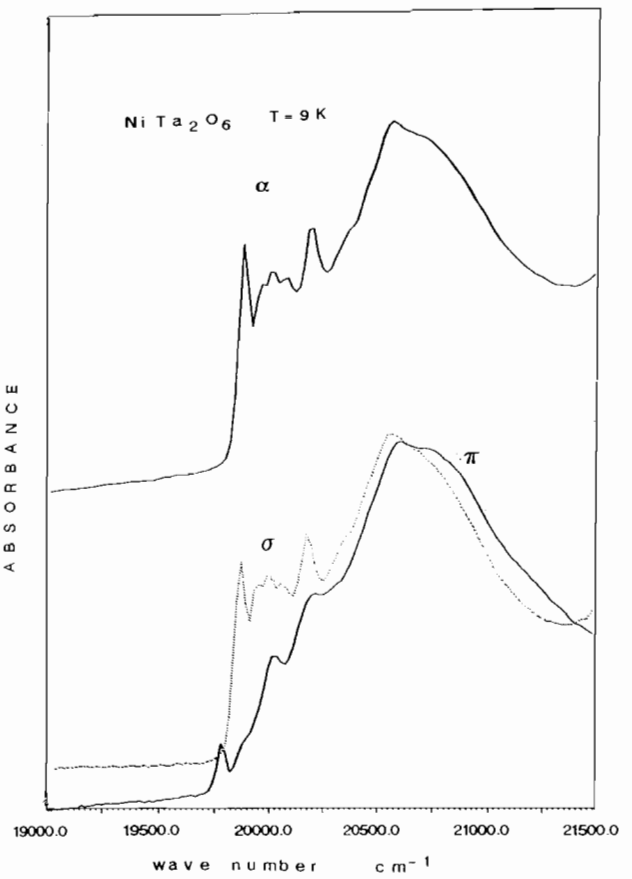


Fig. 7. Weak band system.

considered in connection with each band system is rather large** and their energy separations rather small, it is very difficult to make specific assignments in terms of $D_{2h}^{*}$ states. However from our analysis of the distortion according to the symmetry descent $O_h \rightarrow D_{4h} \rightarrow D_{2h}$, we can expect that the perturbation related to $D_{4h} \rightarrow D_{2h}$ has a greater role with respect to the $O_h \rightarrow D_{4h}$ perturbation. It follows that, in the case where the spin–orbit coupling is relatively smaller with respect to the $D_{4h} \rightarrow D_{2h}$ perturbation, in a first approach an assignment can be made in terms of $D_{2h}$ states by considering only two parameters $\vartheta$ and $\zeta$.

*1st Band system – region 6000–10 500 cm$^{-1}$ (Fig. 4)*

As already pointed out the fact that the $\alpha$ spectrum of the 1st band system is much closer to the $\pi$ spectrum that to the $\sigma$ one shows that the magnetic dipole mechanism is prevailing with respect to the vibronic one. This agrees well with the assignment $^3T_{2g}(1) \leftarrow {}^3A_{2g}(0)$ since this transition is allowed by magnetic dipole mechanism. This interpretation is also supported by the observed rather small variation of intensity in the temperature range 10–50 K, i.e. an opposite behaviour with respect to that expected by a vibronic mechanism.

In $D_{2h}$ symmetry the ground state $^3A_{2g}(0)$ becomes $^3B_{1g}^0$ and the excited state $^3T_{2g}(1)$ separates into $^3A_g + {}^3B_{2g} + {}^3B_{3g}$. Transitions to such components are allowed with the magnetic vector parallel to the axes $z'$, $x'$ and $y'$, respectively (Fig. 2). Taking properly into account the orientations of the two $NiO_6^{n-}$ groups in the unit cell the oscillator strengths vary with the orientation of the magnetic vector according to the expressions

$$
\begin{aligned}
{}^3A_g &\leftarrow {}^3B_{1g}^0 \quad f\alpha\,|\langle {}^3A_g|\mu_{z'}^{MD}|{}^3B_{1g}^0\rangle|^2 \cdot (1-h_c^2)\\
{}^3B_{2g} &\leftarrow {}^3B_{1g}^0 \quad f\alpha\,2|\langle {}^3B_{2g}|\mu_{x'}^{MD}|{}^3B_{1g}^0\rangle|^2 \cdot h_c^2\\
{}^3B_{3g} &\leftarrow {}^3B_{1g}^0 \quad f\alpha\,|\langle {}^3B_{3g}|\mu_{y'}^{MD}|{}^3B_{1g}^0|^2 \cdot (1-h_c^2)
\end{aligned}
$$

where $h_c$ is the cosine of the angle between the magnetic vector and the crystallographic $c$ axis; $\langle {}^3A_g|\mu_{z'}^{MD}|{}^3B_{1g}^0\rangle$, $\langle {}^3B_{2g}|\mu_{x'}^{MD}|{}^3B_{1g}^0\rangle$ and $\langle {}^3B_{3g}|\mu_{y'}^{MD}|{}^3B_{1g}^0\rangle$ are the transition moments; $\mu_{z'}^{MD}$, $\mu_{x'}^{MD}$, $\mu_{y'}^{MD}$ are the components of the magnetic dipole transition operator.

**There are 9 components for each $^3T_1$ or $^3T_2$ excited state and 3 components for the ground state $^3A_{2g}(0)$. In connection with each band system 27 transitions are possible. Most of them are allowed by vibronic mechanism.

TABLE 1. Main features of the band systems; wave numbers of the peaks, shoulders and maxima

| 1st Band system ($\nu$=6000–10500 cm$^{-1}$) | |
|---|---|
| $\alpha$, $\pi$ | $\sigma$ |
| 6720 s.p. | 6720 s.p. |
| 6810 w.sh. | 6810 w.sh. |
| 6900 max. | 6890 s.p. |
| 6935 s.p. | 6935 s.p. |
| 6970 w.max. | 6970 w.max. |
| 7090 | 7090 |
| 7220 | 7220 |
| 7360 | 7340 |
| 7540 | 7540 |
| ~8200 b.max. | 8025 sh. |

| 2nd Band system ($\nu$=11000–16000 cm$^{-1}$) | |
|---|---|
| $\alpha$, $\sigma$ | $\pi$ |
| 11510 | |
| | 11650 |
| 11810 | 11810 |
| 11990 | 11990 |
| | 12120 |
| 12220 sh. | 12220 sh. |
| 12440 max. | |
| | 12580 |
| 12715 | |
| | 12730 |
| | 12880 |
| 12910 max. | |
| | 13305 |
| 13340 | |
| 13530 | |
| 13650 max. | |
| 13820 | |
| | 14335 |
| 14400 s.p. | 14400 s.p. |
| 14580 s.p. | 14580 sh. |

| 3rd Band system ($\nu$=22000–26000 cm$^{-1}$) | |
|---|---|
| $\alpha$, $\sigma$ | $\pi$ |
| 22730 sh. | |
| 23150 max. | |
| | 23310 max. |
| | 23640 |
| | 23895 max. |
| 24125 max. | |
| | 24270 |

| Weak band system ($\nu$=19750–21750 cm$^{-1}$) | |
|---|---|
| $\alpha$, $\sigma$ | $\pi$ |
| | 17790 s.p. |
| 19880 s.p. | 19880 sh. |
| 19960 | |
| 20020 | 20020 |
| 20070 | |
| 20185 s.p. | |
| | 20220 sh. |
| 20370 | |
| 20590 | |
| max. | 20620 |
| 20700 | max. |
| | 20745 |
| 21750 p. | 21750 p. |

p. = peak; s.p. = sharp peak; sh. = shoulder; max. = maximum.

It is clear that we have to expect to observe a band system made of three components, two of them related to the transitions $^3A_g \leftarrow {}^3B^0_{1g}$ and $^3B_{3g} \leftarrow {}^3B^0_{1g}$ with greatest intensity in $\pi$ polarization (where $\vec{H} \perp c$) and one related to $^3B_{2g} \leftarrow {}^3B^0_{1g}$ with greatest intensity in $\sigma$ polarization ($\vec{H} \| c$). Moreover, in the case where the $O_h \rightarrow D_{2h}$ perturbation is sufficiently small, so that one can assume that the above transition moments have approximately the same value (as it holds in $O_h$ symmetry), we have to expect to observe two bands in $\pi$ polarization with almost equal intensity and only one band in $\sigma$ with an almost doubled intensity.

In the observed spectra we have a rather complicated structure. However it is possible to distinguish clearly two bands in $\pi$ polarization in the regions 6700–7800 and 7800–9500 cm$^{-1}$. The first of these in $\sigma$ polarization becomes much more intense whereas the second becomes so weak to appear as a shoulder. On the basis of our above considerations it is easy to deduce that two transitions concern the first region, one of them being $^3B_{2g} \leftarrow {}^3B^0_{1g}$, and only one transition the second region. Thus two alternative assignments can be made

(a) 6700–7800 $^3B_{2g} + {}^3A_g \leftarrow {}^3B^0_{1g}$,

7800–9500 $^3B_{3g} \leftarrow {}^3B^0_{1g}$

or

(b) 6700–7800 $^3B_{2g} + {}^3B_{3g} \leftarrow {}^3B^0_{1g}$

7800–9500 $^3A_g \leftarrow {}^3B^0_{1g}$

From the diagonal elements of the reported ligand field matrices related to the components $^3A_g$, $^3B_{2g}$ and $^3B_{3g}$ of $^3T_{2g}(1)$ (i.e. $\Delta$, $\Delta + 0.5\vartheta$, $\Delta - 0.5\vartheta$) we have two alternative energy orders: $^3B_{2g} < {}^3A_g < {}^3B_{3g}$ if $\vartheta$ is negative, or the reverse $^3B_{3g} < {}^3A_g < {}^3B_{2g}$ if $\vartheta$ is positive**. Since from the observed polarization behaviour of the spectra we have that the transition $^3B_{2g} \leftarrow {}^3B^0_{1g}$ belongs with certainty to the first absorption region 6700–7800 cm$^{-1}$, we can conclude that only the order $^3B_{2g} < {}^3A_g < {}^3B_{3g}$ (i.e. $\vartheta < 0$) and hence assignment (a) is acceptable.

With regard to the three peaks at 6720, 6900 and 6935 cm$^{-1}$ (Fig. 8), we can note that the $\alpha$ polarization is very similar to the $\pi$ one and different from $\sigma$. This proves that also for them the magnetic dipole transition mechanism is predominant. Furthermore their intensity follows exactly the trend of the region 7000–7800 cm$^{-1}$, i.e. much more intense in $\sigma$ polarization with respect to $\pi$ and $\alpha$. The shape of the peaks varies with the lowering of the temperature and, in connection with one of the polarizations, becomes sharper. Specifically

**Such orders are not affected by the value of $\zeta$ because of the large difference between the diagonal elements related to $^3T_{2g}(1)$ and those related to $^3T_{1g}(1)$ and $^3T_{1g}(2)$.

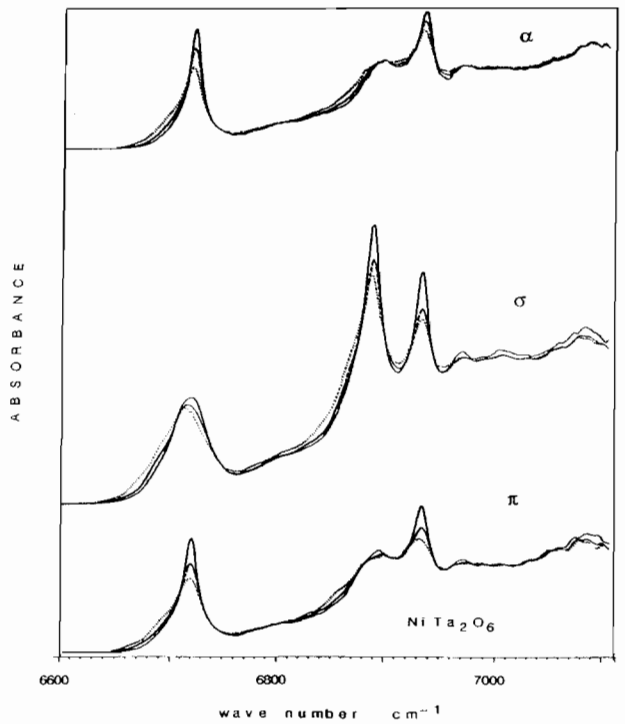


Fig. 8. Temperature behaviour of the peaks at 6720, 6900 and 6935 $cm^{-1}$ of the first band system: —— 10K. – – – 15 K, ··· 20 K.

the first peak is sharper in $\pi$ and $\alpha$, conversely the second peak in $\sigma$. The third peak is sharp in both. However we have to point out that the overall area associated to each peak varies only slightly with temperature within the range 10–50 K. Moreover such variation is regular and smooth even in the interval 10–20 K. We think that this proves that our spectra concern the crystal above the magnetic phase transition*. In order to clarify further the nature of the transitions of the peaks we have also measured the absorption spectrum of $MgTa_2O_6$ (which is isomorph with $NiTa_2O_6$) 'doped' with $Ni^{2+}$. We have verified that the spectrum at 10 K in the region 6600–7800 $cm^{-1}$ presents the same peaks. The main difference is that they shift *c.* 40 $cm^{-1}$ towards lower energy. Particularly the first peak appears at 6680 $cm^{-1}$, the second and the third peak partially merge together with a centre at *c.* 6870 $cm^{-1}$.

On the basis of the above facts we think that an interpretation can be given by considering the spin–orbit coupling as preponderant with respect to the short-range magnetic order interaction. In fact such peaks can be considered the origins of the three components** [10] $\Gamma_1^+$, $\Gamma_3^+$ and $\Gamma_4^+$ in $D_{2h}^*$ *of* $^3B_{2g}$ (Fig. 9) since according to the matrices (1) the $^3B_{2g}$ state must be slightly lower than $^3A_g$. Clearly the higher intensity of the $\sigma$ polarization supports this hypothesis. It is worth pointing out that the energy splitting of the ground state $^3B_{1g}^0$ into the components $\Gamma_1^+$, $\Gamma_2^+$ and $\Gamma_4^+$ is very likely rather small. In fact the mixing with the excited states is certainly low because of the relatively small magnitude of the spin–orbit coupling with respect to the energy differences. Moreover we know from the spin–orbit coupling calculation that such components shift together and approximately to the same extent. Their energy separation is of the order of a few wave numbers and, very reasonably, at 10 K they are almost equally populated. With regard to the states $^3B_{2g}$ and $^3A_g$, they are rather close and overlapping in the same region 6700–7800 $cm^{-1}$. Therefore the components $\Gamma_3^+$ and $\Gamma_4^+$ of $^3B_{2g}$ are strongly mixed with the corresponding ones of $^3A_g$. This mixing cannot occur for $\Gamma_1^+$ because such a component is missing in $^3A_g$. It follows that we have to expect that the two peaks related to $\Gamma_3^+$ and $\Gamma_4^+$ decrease in intensity from the $\sigma$ to $\pi$ polarization to a lesser extent than the peak of $\Gamma_1^+$. This corresponds exactly to what we observe. In particular the peak at 6900 $cm^{-1}$ must correspond

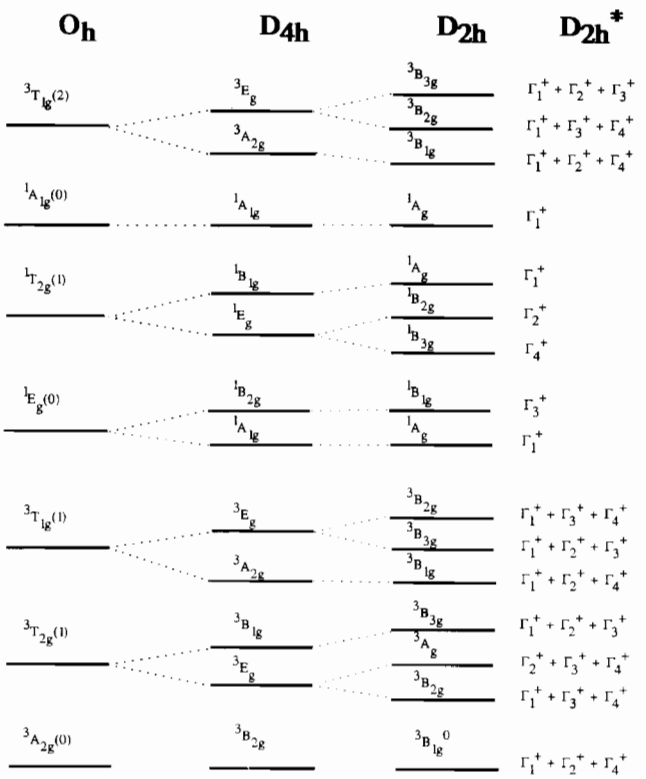


Fig. 9. Removal of the degeneracies in the various symmetries.

*Unfortunately 9 K is the lowest temperature of our cryostat and we did not succeed in detecting the expected antiferromagnetic phase transition in order to check this point.

**In $D_{2h}^*$ we use the conventions of ref. 10.

to $\Gamma_1^+$ and the other two to $\Gamma_3^+$ and $\Gamma_4^+$. From the features of the spectra we cannot deduce the specific correspondence of the latter. From the energy order of our spin–orbit coupling calculations, we know that $\Gamma_3^+$ should correspond to the peak at 6720 $cm^{-1}$ and $\Gamma_4^+$ to 6935 $cm^{-1}$.

*The band systems in the region 11 000–16 000 and 22 000–28 000 $cm^{-1}$ (Figs. 5 and 6)*

We shall examine these two band systems together because they are related to the states $^3T_1(1)$ and $^3T_1(2)$ which have the same symmetry and are strongly mixed. As a consequence we must expect the same transition mechanism and the same polarization behaviour. These points are clearly evident from the spectra. In fact, as already pointed out, for both band systems the $\alpha$ spectrum is much more similar to the $\sigma$ spectrum than to the $\pi$ one. Moreover both present a remarkable variation in intensity with temperature. This shows that the vibronic mechanism is predominant.

With regard to the band system at 11 000–16 000 $cm^{-1}$ one can distinguish three main intervals with different behaviour. Specifically two intervals, approximately in the regions 11 000–12 450 and 12 450–13 100 $cm^{-1}$, appear slightly more intense in the $\pi$ spectrum and present a set of maxima in $\sigma$ polarization. Conversely a third interval in the region 13 100–14 300 $cm^{-1}$ has the highest intensity in the $\sigma$ spectrum and almost disappears in the $\pi$ one. The sharp peaks, one at 14 400 $cm^{-1}$ and another weaker at 14 580 $cm^{-1}$, have to be considered separately because in $O_h$ they correspond to the transition $^1E_g(0) \leftarrow {}^3A_{2g}(0)$.

In the band system at 22 000–28 000 $cm^{-1}$ we note two maxima at 23 150 and 24 100 $cm^{-1}$, and one shoulder at *c.* 22 550 $cm^{-1}$. The part of the band system related to the two maxima is clearly much more intense in $\pi$ polarization. Conversely the shoulder appears only in $\sigma$ polarization.

Each state, $^3T_{1g}(1)$ and $^3T_{1g}(2)$, in $D_{2h}$ symmetry splits into three components: $^3B_{1g} + {}^3B_{2g} + {}^3B_{3g}$.

The vibrational spectra of $NiTa_2O_6$ have been widely investigated [11]. From such spectra there is clear evidence that the oxygen atoms are much more strongly bound to the Ta atoms than to the Ni atoms. However, if we consider only the $O_h$ internal vibrational modes of the $NiO_6^{n-}$ system which can participate in the vibronic transition mechanism, we have to deal with two $\tau_{1u}$ modes and one $\tau_{2u}$ mode. Such modes decompose in $D_{2h}$ symmetry as follows:

$$\tau_{1u} = b_{1u} + b_{2u} + b_{3u} \qquad \tau_{2u} = a_u + b_{2u} + b_{3u}$$

In Table 2 we give the $D_{2h}$ vibrational modes which can allow transitions to the triplet states. The modes therewith reported relative to the electric vector orientation $\vec{E} \perp c$ (where the transition operator belongs to either $B_{1u}$ or $B_{2u}$) determine the intensities of the transitions in the $\sigma$ spectrum and those with $\vec{E} \parallel c$ (where the transition operator belongs to $B_{3u}$) the intensities in the $\pi$ spectrum. It follows that, if the $\tau_{1u}$ modes are the most effective, the transitions $^3B_{2g} \leftarrow {}^3B_{1g}^0$ must be relatively weaker when $\vec{E} \parallel c$ because they can occur only by means of the $a_u$ mode which is missing in $\tau_{1u}$. Conversely if the $\tau_{2u}$ mode is the most effective the transitions $^3B_{3g} \leftarrow {}^3B_{1g}^0$ have to be weaker when $\vec{E} \parallel c$ because they can occur only by means of the $b_{1u}$ mode which is not a component of $\tau_{2u}$.

TABLE 2. Vibrational modes in $D_{2h}$ symmetry which can be active in the vibronic transitions

| $O_h$ | $D_{2h}$ | $E \perp c$ ($B_{1u}$, $B_{2u}$) | $E \parallel c$ ($B_{3u}$) |
|---|---|---|---|
| $^3T_{2g} \leftarrow {}^3A_{2g}$ | $^3A_g \leftarrow {}^3B_{1g}$ | $a_u$, $b_{3u}$ | $b_{2u}$ |
| | $^3B_{2g} \leftarrow {}^3B_{1g}$ | $b_{2u}$, $b_{1u}$ | $a_u$ |
| | $^3B_{3g} \leftarrow {}^3B_{1g}$ | $b_{3u}$, $a_u$ | $b_{1u}$ |
| $^3T_{1g} \leftarrow {}^3A_{2g}$ | $^3B_{1g} \leftarrow {}^3B_{1g}$ | $b_{1u}$, $b_{2u}$ | $b_{3u}$ |
| | $^3B_{2g} \leftarrow {}^3B_{1g}$ | $b_{2u}$, $b_{1u}$ | $a_u$ |
| | $^3B_{3g} \leftarrow {}^3B_{1g}$ | $b_{3u}$, $a_u$ | $b_{1u}$ |

In order to make the assignments it is convenient to examine the matrices (1) previously reported. First of all we have to point out that in $O_h$ symmetry the diagonal elements have rather close values (e.g. with $10Dq = 7600$ $cm^{-1}$ and $B = 850$ $cm^{-1}$ we have $\Delta + 12B = 17\,800$ $cm^{-1}$ and $2\Delta + 3B = 17\,750$ $cm^{-1}$) and their off-diagonal element relatively large ($6B = 5100$ $cm^{-1}$). This implies a strong mixing of the two states. It follows that the large energy separation between the two band systems is mainly due to the off-diagonal element.

In $D_{2h}$ symmetry each $^3T_{1g}$ state splits into the components $^3B_{1g}$, $^3B_{2g}$, $^3B_{3g}$ and, because of the large role of the off-diagonal element between $^3T_{1g}(1)$ and $^3T_{1g}(2)$, the related energy separations depend remarkably on both $\vartheta$ and $\zeta$. From the reported matrices (1) one can deduce that the half-plane spanned by $\vartheta/B < 0$ and $\zeta/B$ can be divided into three regions (Fig. 10) characterized by a different energy order of the components of the two band systems as follows

Band system 11 000–16 000 $cm^{-1}$

| | |
|---|---|
| Region (a) | $^3B_{3g} < {}^3B_{1g} < {}^3B_{2g}$ |
| Region (b) | $^3B_{2g} < {}^3B_{1g} < {}^3B_{3g}$ |
| Region (c) | $^3B_{3g} < {}^3B_{1g} < {}^3B_{2g}$ |

Band system 22 000–28 000 $cm^{-1}$

| | |
|---|---|
| Region (a) | $^3B_{2g} < {}^3B_{1g} < {}^3B_{3g}$ |
| Region (b) | $^3B_{3g} < {}^3B_{1g} < {}^3B_{2g}$ |
| Region (c) | $^3B_{3g} < {}^3B_{1g} < {}^3B_{2g}$ |

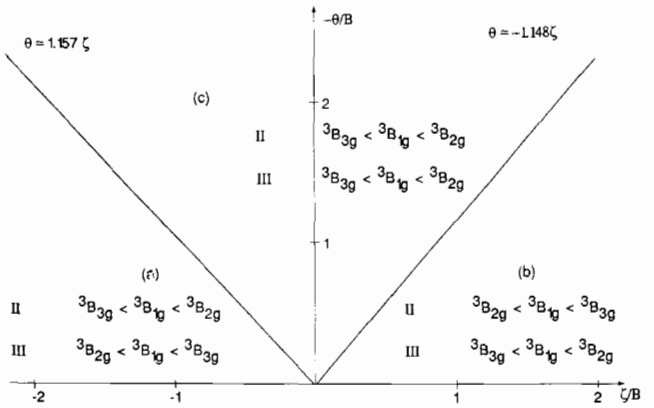


Fig. 10. Energy order of the components of the $^3T_{1g}$ excited states (II: band system 11000–16000 $cm^{-1}$; III: band system 22000–28000 $cm^{-1}$) as function of the parameters $\zeta/B$ and $-\theta/B$.

TABLE 3.

| | | Case $\zeta<0$ region (a) | Case $\zeta>0$ region (b) |
|---|---|---|---|
| Band system II | 11600–12450 $cm^{-1}$ | $^3B_{3g} \leftarrow {}^3B^0_{1g}$ | $^3B_{2g} \leftarrow {}^3B^0_{1g}$ |
| 11000–16000 $cm^{-1}$ | 12450–13100 $cm^{-1}$ | $^3B_{1g} \leftarrow {}^3B^0_{1g}$ | $^3B_{1g} \leftarrow {}^3B^0_{1g}$ |
| | 13100–14300 $cm^{-1}$ | $^3B_{2g} \leftarrow {}^3B^0_{1g}$ | $^3B_{3g} \leftarrow {}^3B^0_{1g}$ |
| Band system III | 22500 $cm^{-1}$ (sh) | $^3B_{2g} \leftarrow {}^3B^0_{1g}$ | $^3B_{3g} \leftarrow {}^3B^0_{1g}$ |
| 22000–28000 $cm^{-1}$ | 23150 $cm^{-1}$ (max) | $^3B_{1g} \leftarrow {}^3B^0_{1g}$ | $^3B_{1g} \leftarrow {}^3B^0_{1g}$ |
| | 24100 $cm^{-1}$ (max) | $^3B_{3g} \leftarrow {}^3B^0_{1g}$ | $^3B_{2g} \leftarrow {}^3B^0_{1g}$ |

In regions (a) and (b) of Fig. 10 the symmetry of the highest component of the band system at 11 000–16 000 $cm^{-1}$, i.e. $^3B_{2g}$ and $^3B_{3g}$, respectively, is the same as the lowest component of the band system at 22 000–28 000 $cm^{-1}$. Moreover the component $^3B_{1g}$ is between $^3B_{2g}$ and $^3B_{3g}$.

Since from our spectra we have evidence that the interval 13 000–14 300 $cm^{-1}$ of the band system at 11 000–16 000 $cm^{-1}$, which very likely corresponds to the highest component, behaves with regard to polarization exactly as the shoulder at *c.* 22 550 $cm^{-1}$, which is the lowest component of the band system at 22 000–28 000 $cm^{-1}$, we can deduce that $NiTa_2O_6$ is either in region (a) or (b). Therefore see the alternative assignments possible in Table 3.

The assignments connected to region (a), i.e. $\zeta<0$, correspond to the cases in which the $\tau_{1u}$ modes are the most effective. Conversely the assignments related to region (b), i.e. $\zeta>0$, correspond to the cases in which the $\tau_{2u}$ modes are most effective.

From the spectra we have no elements to verify which of the above assignments is the correct one. We are more inclined to the assignment of region (a) for the following reasons: it corresponds to the case with the $\tau_{1u}$ modes as more effective which we think more likely; a negative value of $\zeta$ is more consistent with a ligand field treatment in which one takes into account the $D_{4h} \rightarrow D_{2h}$ distortion in terms of a point-charge model.

The behaviour of the intensity of the peaks at 14 400 and 14 580 $cm^{-1}$ due to the transition $^1E_g(0) \leftarrow {}^3A_{2g}(0)$ can be explained by considering the possible mixing with the nearby state due to the spin–orbit coupling. In fact in $D^*_{2h}$ symmetry the state $^1E_g(0)$ splits into $\Gamma_1^+ + \Gamma_3^+$. The component $^3B_{2g}$ of $^3T_{1g}(1)$ decomposes further into $\Gamma_1^+ + \Gamma_3^+ + \Gamma_4^+$ and the component $^3B_{3g}$ into $\Gamma_1^+ + \Gamma_2^+ + \Gamma_3^+$. Whichever component $^3B_{2g}$ or $^3B_{3g}$ is related to the interval at 13 100–14 300 $cm^{-1}$, both have as sub-components $\Gamma_1^+$ and $\Gamma_3^+$ which can contribute to the intensity of the peaks. In the spectra we observe that the intensity of the peaks follows closely the behaviour of the nearby interval at 13 100–14 300 $cm^{-1}$. Specifically they are much more intense in $\sigma$ polarization.

*Weak band system—region 19 750–21 750 $cm^{-1}$ (Fig. 7)*

The spectrum of $NiTa_2O_6$ in the region 19 750–21 750 $cm^{-1}$ has a weak band system which cannot correspond to any of the components of $^3T_{1g}(2)$ because it is too weak. Very likely it has to be assigned to $^1T_{2g}(1) \leftarrow {}^3A_{2g}(0)$. The state $^1T_{2g}(1)$ in $D^*_{2h}$ splits into $\Gamma_1^+ + \Gamma_2^+ + \Gamma_4^+$. Its closest band of triplet is the shoulder at 22 550 $cm^{-1}$ assigned above as $^3B_{2g} \leftarrow {}^3B^0_{1g}$ or $^3B_{3g} \leftarrow {}^3B^0_{1g}$. The state $^3B_{2g}$ in $D^*_{2h}$ subdivides as $\Gamma_1^+ + \Gamma_3^+ \Gamma_4^+$ and two of them, i.e. $\Gamma_1^+$ and $\Gamma_4^+$, can mix with the corresponding components of $^1T_{2g}(1)$. Similarly the state $^3B_{3g}$ subdivides as $\Gamma_1 + \Gamma_2^+ + \Gamma_3^+$ and $\Gamma_1^+$ and $\Gamma_2^+$ can mix with the corresponding components of $^1T_{2g}(1)$ (Fig. 9) This means that whichever is the state associated to the shoulder, the intensity of the weak band system must follow the behaviour of the shoulder at 22 550 $cm^{-1}$ as polarization. This is really observed in the part of the band system between 19 750 and 20 300 $cm^{-1}$. In fact it is rather more intense in $\sigma$ polarization. However there is a remaining part in the range 20 300–21 500 $cm^{-1}$ which varies only slightly with polarization and it is rather difficult to interpret. A possible hypothesis is that it corresponds to the other component $\Gamma_2^+$ of $^1T_{2g}(1)$ which borrows intensity from the corresponding components of the other nearby states of $^3T_{1g}(2)$.

This part of the spectrum presents also a weak peak at 21 750 $cm^{-1}$ (Fig. 6) well separated from the other parts and very close to the band system at 22 000–28 000 $cm^{-1}$. As already stated,such a peak corresponds to $^1A_g[^3A_{2g}(0)] \leftarrow {}^1B^0_{1g}$.

*Ligand field calculations*

A ligand field calculation carried out by considering all the parameters is not very meaningful because their

number is too large. Therefore we have carried out several ligand field calculations with different extents of parametrization. In a first approach we have neglected all the parameters representative of the $O_h \rightarrow D_{4h} \rightarrow D_{2h}$ distortions and calculated the values of $10Dq$, $B$ and $C$ which give the best fit of the centres of the band systems (Table 4, columns $A_1$ and $A_2$).

In a second approach keeping the above values of $10Dq$, $B$ and $C$ we have calculated the parameters $\vartheta$ and $\zeta$ on the basis of the best fit of the centres of the ranges reported in Table 3 (column B) assumed as corresponding to the transitions $D_{2h}$. In this case we have considered the previously discussed alternative assignments (columns $C_1$ and $D_1$). The results are reported in columns $C_2$ and $D_2$.

Finally we have carried out two calculations by including the spin–orbit coupling with $\xi = 600$ cm$^{-1}$ and using the same ligand field parameters of columns $C_2$ and $D_2$ of Table 3. All the ligand field states have been considered. We do not report the results because they agree with the interpretation already made by neglecting the spin–orbit coupling and, in addition, do not allow more specific assignments.

Calculations including the parameters $\eta$ and $\epsilon$ representative of the $O_h \rightarrow D_{4h}$ distortion have been also done. The improvement of the results is only slight and meaningless.

## Conclusions

The absorption spectrum of the system $NiTa_2O_6$ within the range 6000–28 000 cm$^{-1}$ concerns electronic transitions essentially related to the $Ni^{2+}$ ions. Although there is evidence of some magnetic order [8] and hence of interaction among the $Ni^{2+}$ ions, the main features of the spectra down to 10 K can be interpreted as due to transitions localized on single $NiO_6^{n-}$ groups. In fact the various regions of absorption correspond to band systems which can be related to specific ligand field transitions on the $Ni^{2+}$ ion.

TABLE 4. Transition assignments

| | $O_h$ | | | $D_{2h}$ | | | |
|---|---|---|---|---|---|---|---|
| | Estimated centres (cm$^{-1}$) | $\nu_{calc}$ (cm$^{-1}$) | Observed band ranges (cm$^{-1}$) | Case (a) $\zeta < 0$ | | Case (b) $\zeta > 0$ | |
| | | | | Assignment | $\nu_{calc}$ (cm$^{-1}$) | Assignment | $\nu_{calc}$ (cm$^{-1}$) |
| | $A_1$ | $A_2$ | B | $C_1$ | $C_2$ | $D_1$ | $D_2$ |
| $^3A_{2g}(0)$ | 0 | 0 | | $^3B_{1g}^0$ | 0 | $^3B_{1g}^0$ | 0 |
| $^3T_{2g}(1)$ | 7650 | 7600 | 6700–7600<br>7000–7800<br>7800–9500<br>(max 8250) | $^3B_{2g}$<br>$^3A_g$<br>$^3B_{3g}$ | 7429<br>7661<br>7754 | $^3B_{2g}$<br>$^3A_g$<br>$^3B_{3g}$ | 7428<br>7662<br>7843 |
| $^3T_{1g}(1)$ | 12950 | 12675 | 11500–12700<br>12700–13300<br>13300–14300<br>(max 13700) | $^3B_{3g}$<br>$^3B_{1g}$<br>$^3B_{2g}$ | 11685<br>12775<br>13922 | $^3B_{2g}$<br>$^3B_{1g}$<br>$^3B_{3g}$ | 12179<br>12777<br>13297 |
| $^1E_g(0)$ | 14500 | 13723 | 14400<br>14580 | $^1A_g$<br>$^1B_{1g}$ | 13596<br>13700 | $^1A_g$<br>$^1B_{1g}$ | 13602<br>13700 |
| $^1T_{2g}(1)$ | 20600 | 20921 | 19750–21400 | $^1A_g$<br>$^1B_{2g}$<br>$^1B_{3g}$ | 20855<br>21045<br>21090 | $^1A_g$<br>$^1B_{2g}$<br>$^1B_{3g}$ | 20782<br>20536<br>21104 |
| $^1A_{1g}(0)$ | 21750 | 21987 | 21750 | $^1A_g$ | 22185 | $^1A_g$ | 22333 |
| $^3T_{1g}(2)$ | 23300 | 22875 | 22200–22800<br>(shoulder)<br>22650–23650<br>(max 23150)<br>23650–24950<br>(max 24200) | $^3B_{2g}$<br>$^3B_{1g}$<br>$^3B_{3g}$ | 22342<br>22958<br>23534 | $^3B_{3g}$<br>$^3B_{1g}$<br>$^3B_{2g}$ | 21777<br>22960<br>24150 |

$A_1$: estimated baricentres of the band systems. $A_2$: transitions calculated in $O_h$ symmetry with $\Delta = 7600$ cm$^{-1}$, $B = 850$ cm$^{-1}$, $C/B = 4.38$. B: band ranges estimated from the shape of the band systems. $C_1$ and $D_1$: alternative assignments. $C_2$ and $D_2$: transition energies calculated with $\Delta = 7600$ cm$^{-1}$, $B = 850$ cm$^{-1}$, $C/B = 4.38$ and respectively (a): $\vartheta = -360$ cm$^{-1}$, $\zeta = -1000$ cm$^{-1}$ and (b): $\vartheta = -420$ cm$^{-1}$, $\zeta = 1010$ cm$^{-1}$.

The intensity of the bands varies with the polarization of the light. Such variation can be interpreted as the sum of the behaviours of the two $NiO_6^{n-}$ groups of the unit cell. The behaviour of each $NiO_6^{n-}$ group can be explained on the basis of the site symmetry $D_{2h}$. The $O_h \rightarrow D_{2h}$ perturbation can be decomposed into two contributions related to the steps $O_h \rightarrow D_{4h}$ and $D_{4h} \rightarrow D_{2h}$. We appear to have clear evidence that the second contribution is preponderant. In fact by considering only the latter we are able to explain most of the features. Conversely the hypothesis of the $O_h \rightarrow D_{4h}$ perturbation as preponderant gives completely inadequate results.

In particular we note that:

- The polarization behaviour shows that the first band system in the region 6000–10 500 $cm^{-1}$ corresponds to electronic transitions which occur mainly by magnetic dipole mechanism. This mechanism has already been found in similar systems [6]. However we think that in $NiTa_2O_6$ the evidence is more clear.
- From the polarization behaviour we know that the band systems at 11 000–15 600 and 20 000–28 000 $cm^{-1}$ correspond to electronic transitions which occur by electric dipole mechanism. The remarkable variation of the intensity with temperature proves the vibronic character of the transitions.
- In each intense band system one can identify three main intervals corresponding to overlapping bands. Two alternative assignments can be given by assuming the $D_{4h} \rightarrow D_{2h}$ distortion as predominant. The alternative depends on which of the vibrational modes $\tau_{1u}$ or $\tau_{2u}$, is more effective.
- The three peaks at the beginning of the first band system can be explained as the origins of the components $\Gamma_1^+$, $\Gamma_3^+$ and $\Gamma_4^+$ of $^3B_{2g}[^3T_{2g}(1)]$ when the spin–orbit coupling is taken into account.

**Acknowledgement**

Research done within the 'Progetto Finalizzato Materiali Speciali per Tecnologie Avanzate' of the Italian National Research Council (C.N.R.).

**References**

1 R. Borromei, G. Ingletto, L. Oleari and P. Day, *J. Chem. Soc., Faraday Trans. II, 77* (1981) 2249.
2 R. Borromei, G. Ingletto, L. Oleari and P. Day, *J. Chem. Soc., Faraday Trans. II, 79* (1983) 847.
3 R. Borromei and E. Cavalli, *Phys. Status Solidi (b), 123* (1984) 679.
4 A. Belletti, R. Borromei, R. Cammi and E. Cavalli, *Phys. Status Solidi (b), 163* (1991) 281.
5 R. Cammi, L. Oleari and C. Oleari, *II Nuovo Cimento, 8D* (1986) 1.
6 J. Ferguson, H. J. Guggenheim, H. Kamimura and Y. Tanabe, *J. Chem. Phys., 42* (1965) 775.
7 H. Muller-Buschbaum and R. Wichmann, *Z. Anorg. Allg. Chem., 536* (1986) 15.
8 M. Takano and T. Takada, *Mater. Res. Bull., 5* (1970) 449.
9 D. S. McClure, *Electronic Spectra of Molecules and Ions in Crystals,* Academic Press, New York, 1959.
10 C. F. Koster, J. O. Dimmock, R. G. Wheeler and H. Statz, *Properties of the Thirty-two Point Groups,* MIT Press, Cambridge, MA, 1963.
11 E. Husson, Y. Repelin and H. Brusset, *Spectrochimica Acta, Part A, 35* (1979) 1177; *J. Solid State Chem., 33* (1980) 375.